Chapter

Methodology for Composite Blades Testing: From UAVs to Mega-Large Structures

Goran Vorotović, Jela Vorotović, Nebojša Petrović, Nikola Davidović, Đorđe Novković and Pavle Petrović

Abstract

The use of composite rotor blades in the domains of micro-aircraft, aircraft for the transport of goods and passengers, for military purposes, as well as in the domain of wind turbines represents one of the most significant aspects in the problems of aerodynamics and energy efficiency, especially from the aspect of safety. The real use of composite blades whose traction-dynamic, lift, and thrust dynamic characteristics in real conditions of exploitation are directly dependent on complex loads of a static and dynamic nature requires a comprehensive laboratory analysis according to appropriate methodological principles. This chapter presents the results of multi-decade research aimed at identifying and verifying a unique methodology for testing composite blades on examples of UAV blades, blades exposed to extreme conditions of exploitation, as well as blades used for electricity generation. It is interesting to note that the methodology, regardless of the dimensions of the blades and their purpose, is practically applicable to all cases of blade use in the earth's atmosphere, where obtained test results realistically describe the complex behavior of the blades in real exploitation conditions.

Keywords: propeller, traction-dynamic characteristics, oscillations, acquisition, dynamics

1. Introduction

Composite materials represent a combination of two or more materials with different physical and chemical properties on a macroscopic scale, with the aim of forming a new usable material. Composite, in fact, is a material consisting of an elastic matrix, which ensures the homogeneity and workability of the composite and filling, which ensures the rigidity and strength of the structure. The characteristics of the matrix are good shear resistance, low specific gravity, and good workability. The characteristics of the filling (reinforcing fibers) are high strength, high modulus of elasticity, and low specific weight. Based on these properties, we can come to the specifics of the

composite, namely: strength much higher than the strength of the matrix, modulus of elasticity much higher than the modulus of the matrix, and specific weight approximately the same as the weight of the matrix.

It has been shown that the use of composite materials, for the supporting elements of the construction of aviation structures, provides a number of advantages compared to classic aviation materials. These advantages can be in terms of carrying capacity and construction:

- the transmission of forces through a larger number of fibers and the application of simultaneous polymerization of several structural elements in one tool enables obtaining a tough construction, which has a relatively high load capacity even after partial damage,

- the basic structure can be made from a small number of assemblies and subassemblies,

- in accordance with the previous one, the number of mechanical connecting elements can be reduced;

 or in terms of servicing and exploitation:

- composites have high anti-corrosion properties,

- have low thermal conductivity,

- the finished surfaces are aerodynamically clean and do not require subsequent treatment,

- the process of overhauling the structure is quite simple and does not require special conditions [1, 2].

Composite materials, in addition to high strength and rigidity, are characterized by fatigue and vibration resistance. These are properties that directly affect the extension of the exploitation life of elements made of these materials. Composites are characterized by the retention of a high percentage of static strength, both unidirectional and transversely stacked laminates. In addition to all this, they are characterized by low density, which directly affects the reduction of the mass of the structure. How much this reduction will be depending on the complexity of the structure, its dimensions, and the intensity of the load.

The design of rotor blades is a balanced integration of aerodynamics, structural analysis and dynamics, choice of different types of composite materials, production technology, and overall economy.

The design of modern rotor includes choice of blade number, airfoil, chord, and twist distribution. Additional criteria are reliability, noise, and esthetic considerations. One of the important requirements when designing a propeller is the maximum reliability of the structure in all modes of exploitation. Such optimization requires the inclusion of all parameters through aerodynamic and structural modeling and the adoption of all major components of the system that includes the use of propellers.

Following is the methodology developed in a course of 40 years of testing of blades of various purposes. This methodology can be used when designing a new rotor blade or

to check the quality of the blade of a known form and shape. These tests include performance testing, fatigue, and structural testing like the one presented in [3–5].

2. Performance testing

The performance testing represents the determination of the traction dynamic characteristics of a propeller, i.e., its thrust force and torque in conjunction with number of revolutions per minute [6].

The test bench for testing the traction-dynamic properties of propellers (1) is built of aluminum profiles (**Figure 1**). This test bench can safely test propellers with diameters of up to 550 mm. The power group comprises one 250 W alternating current motor (2) controlled by a torus precise alternating current regulator (8) with a voltage range of 0–300 V. The torus regulator guarantees that the operational voltage changes continuously. The motor is situated in an aerodynamic formwork constructed of aluminum, which is supported by an aerodynamic pylon (3). A precise scale (7), which is an
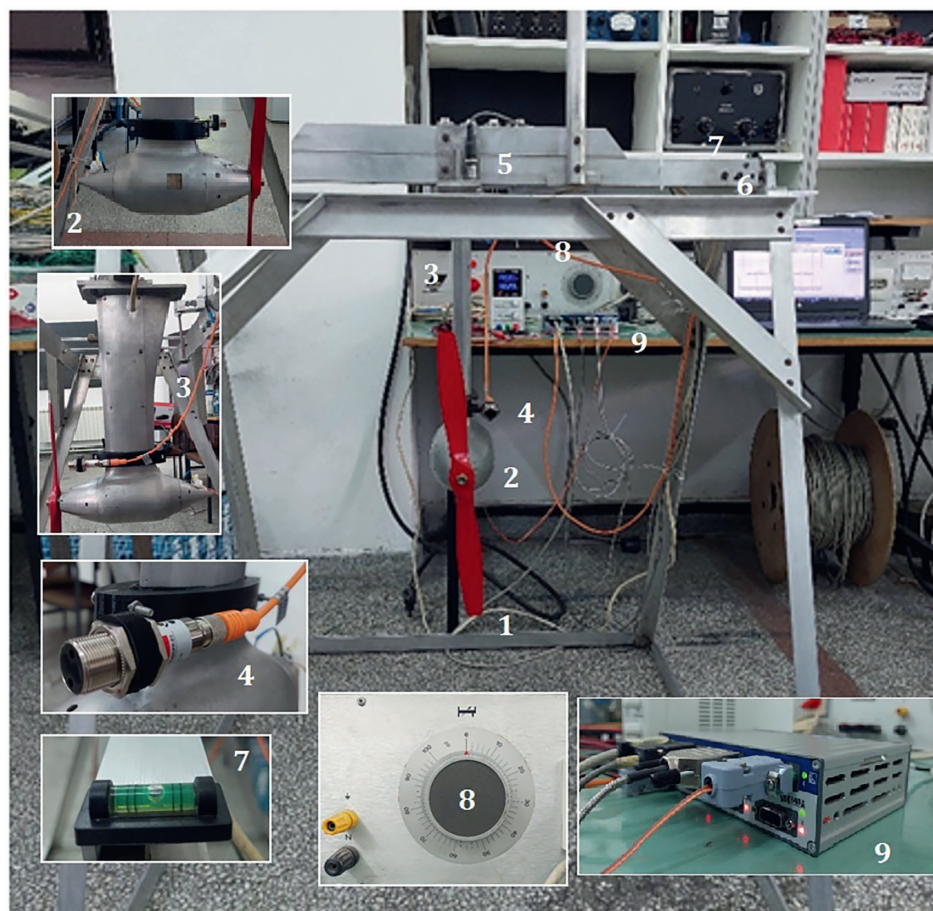

Figure 1.
Experimental setup for traction-dynamic characteristics evaluation.

integrated component, is utilized to finely adjust the propeller's zero balance point, since this test bench can be used for testing of propellers of wide range of diameters, which are of different geometry, hence of different mass. The propeller is mounted on the test bench using a conical holder on the driving shaft that is locked with a self-locking nut.

Propeller's trust is obtained via a consol-type force transducer presented in **Figure 2**. The thrust of the propeller is consequence of its rotation. Number of revolutions per minute of the propeller is obtained with the use of an optical digital encoder LANELO PR18-BC40DPR-E2 (position (4) in **Figure 1**). The encoder is mounted on the aerodynamic support that follows the contour of the pylon and enables the adjustment of the encoder's position in reference to the propeller, if there is the necessity to adjust the measurement response. The propeller's torque is measured via two strain gauges of 120 Ω that are mounted on a special console support that is designed and produced for the purpose of torque measurement. Strain gauge that is used for thrust force measurement is connected to the acquisition device with a Wheatstone full-bridge, while the strain gauges used for torque measurement are connected via Wheatstone half-bridge.

Any propeller imbalance during the test is noticed by the vibration detection system. It consists of two accelerometers (**Figure 3**) that are mounted on different parts of the test bench. One of the accelerometers (Monitran MTN/7100-50, position (6) in **Figure 1**) is placed on a fixed part of the structure, while the other one (HBM 1-B12/200, position (5) in **Figure 1**) is mounted on the moving part of a test bench that is under impact of the thrust force of the propeller. In the case of a resonance of these two sensors, the experiment is automatically terminated.

An eight-channel data acquisition unit QuantumX MX840A is used for measurements that enables 20,000 measurements per second per channel with 24-bit resolution. All 8 A/D converters work synchronously and monitor the transformation of physical quantities into a digital signal in real time. QuantumX contains a LAN and FireWire bus in order to deliver acquired data to the acquisition computer, as well as for expanding the number of measurement points by direct connection to several quantum devices. Before the measurements take place, output of force and torque sensors are set to zero, in order to prevent accumulation error that could emerge on these sensors.

Confirmation of the proposed methodology was carried out by measurements on the propeller shown in **Figure 4**, with a diameter of 420 mm, reference pitch angle at 3/4*D,* and Clark-Y airfoil.

Measurements confirm that the thrust is a square function of the RPM, as is predicted by theory. With increase in RPM the thrust is increased, since the propeller blades rotate faster, thus increasing the air mass flow rate flowing against them. The
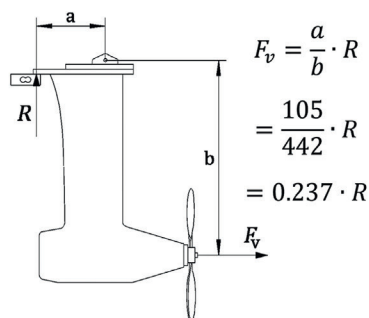

$$F_v = \frac{a}{b} \cdot R$$

$$= \frac{105}{442} \cdot R$$

$$= 0.237 \cdot R$$

Figure 2.
Thrust measurement setup.

Figure 3.
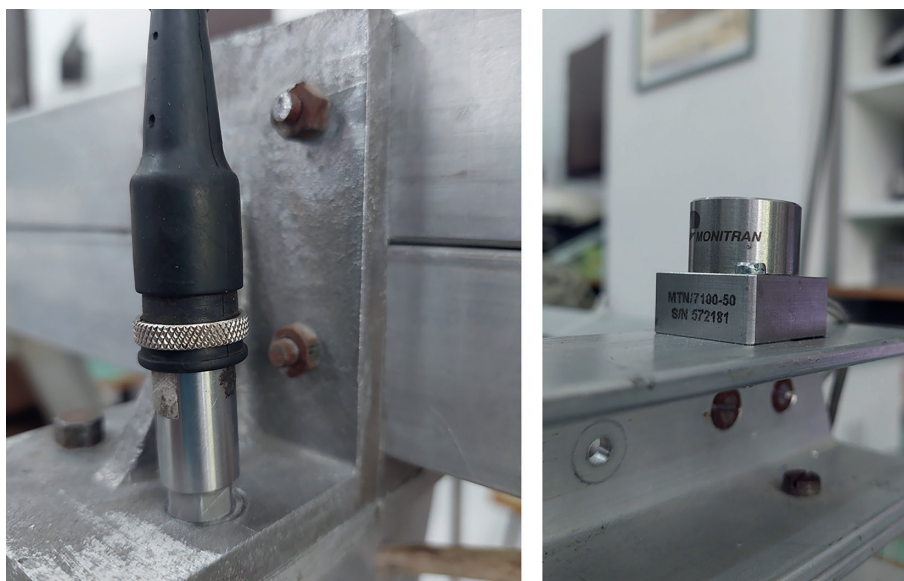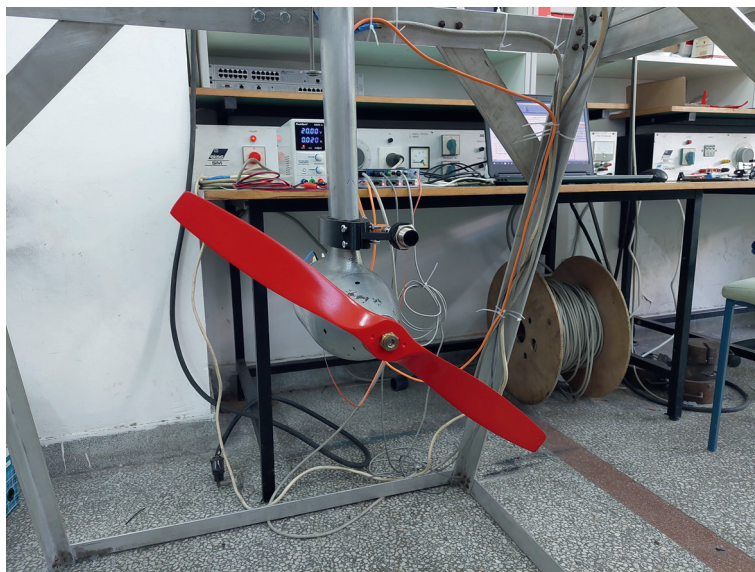*Accelerometers (HBM and Monitran).*

Figure 4.
Propeller ready for testing.

consequence of this is the increase of the forward load applied to the propeller that acts as a moving force forward. Due to the construction of the test bench and the position of the load cell, this motion is restricted by the load cell itself. Hence, the load cell is 'perceiving' the thrust acting on the propeller.

Figure 5 on the right illustrates how the resistance torque varies with RPM. There is a slightly higher variability in the measured values, with a correlation coefficient
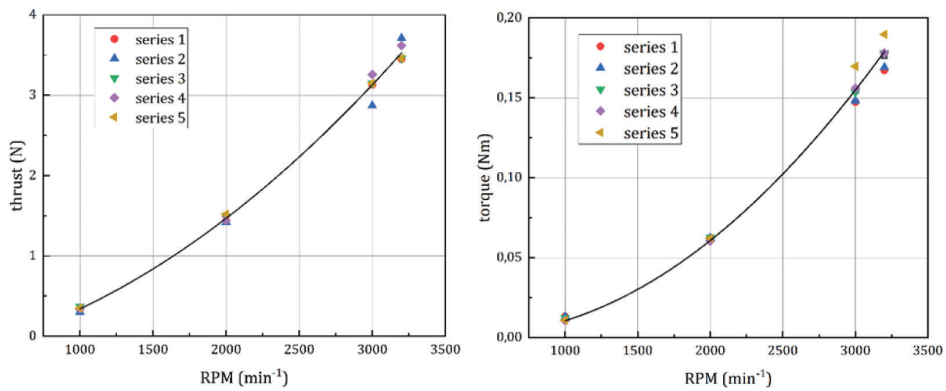
Figure 5.
Thrust force and torque for different values of RPM.

of 0.96. The primary discrepancy in the results occurs at higher RPMs. This variation in torque values is likely due to insufficient stiffness in the console support where the measuring tapes are positioned, leading to increased vibration in the test bench. Consequently, these findings further indicate the quality of the tested propeller.

Figure 6 presents the time dependencies of the signals from the traction force sensor and the resistive torque sensor across all RPMs and measurement series. A clear
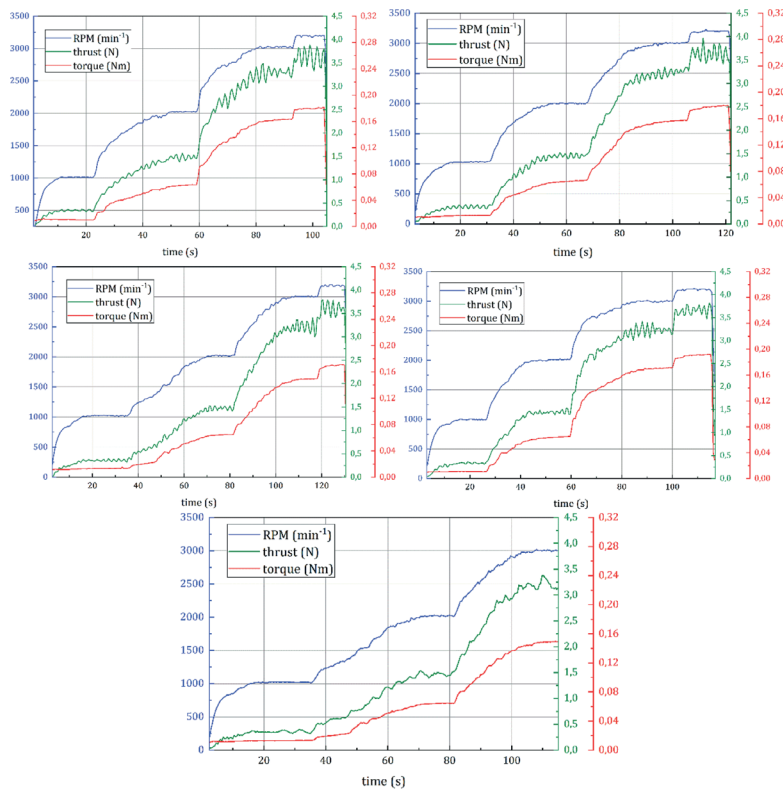

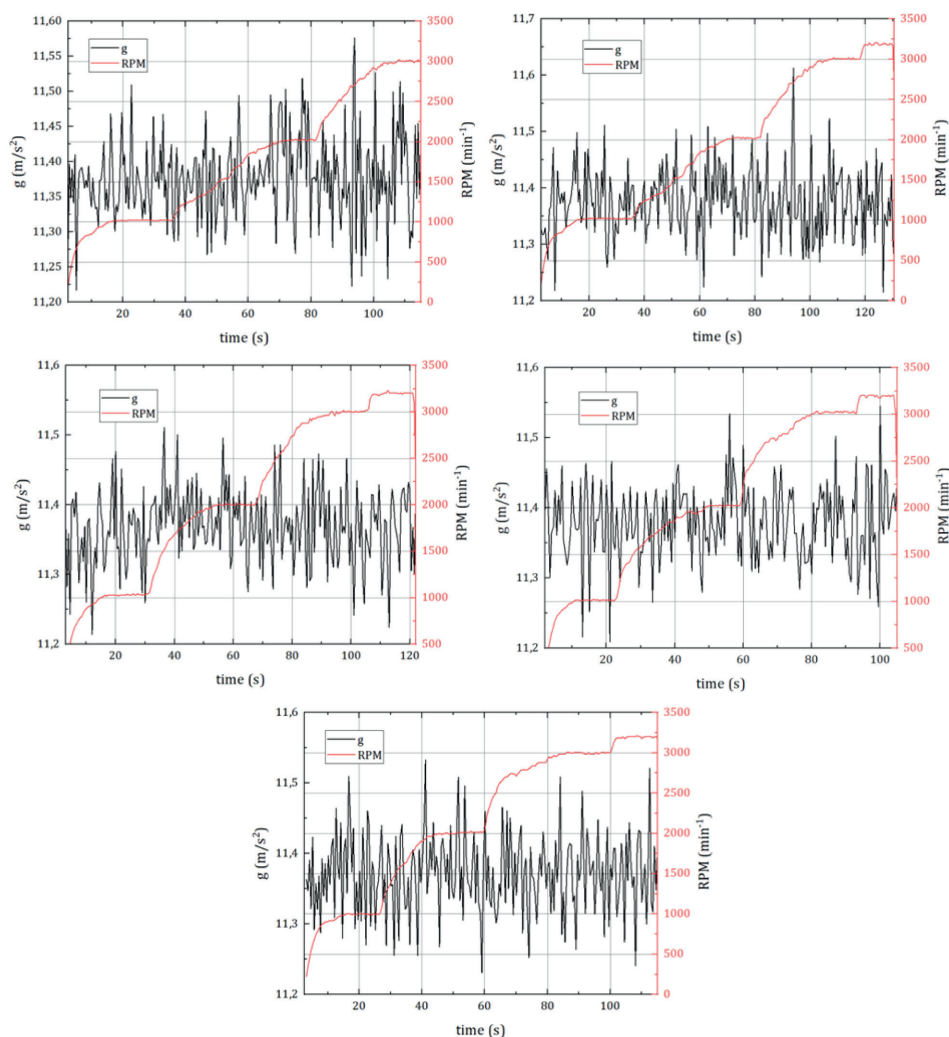**Figure 6.**
Time evolution of RPM, thrust, and torque.

Figure 7.
Signal from accelerometer with the change in RPM.

trend shows that both traction force and torque values track changes in the number of revolutions. Additionally, there is instability in the traction force sensor signal at RPMs exceeding 2000 min^{-1}, which is attributed to increased vibrations on the test bench caused by the imperfections in the tested propeller.

Figure 7 displays the comparative time dependence diagrams of the signals from the vibration transmitter and the optical encoder used to measure the propeller's RPM. In all measurement series, increased vibrations are evident at 2000 min^{-1}, indicating asymmetry in the tested propeller.

3. Mechanical testing

The mechanical testing implies rigidity (flexural and torsional) testing, fatigue testing, and bump test. These series of testing are performed on a single test bench

that has two parts. In one part, we can perform rigidity testing, while the other part serves for fatigue and bump testing.

3.1 Rigidity tests

The program for rigidity testing of the composite rotor blade is defined by standard IEC 61400-2 [7]. The purpose of this testing is to define the rigidity of the rotor blade and to determine the maximum force or coupling of forces that cause the failure of the rotor blade as well as the spot of the failure.

The holder for the blade that is meant to be subjected to rigidity testing constitutes of extremely rigid specious grid made of steel C and L profiles that are mutually connected by bolt links. The link between the rotor blade and the holder is accomplished through 30 mm board and by bolts M8 of 8.8 quality. The rotor blade is mounted on the structure at the angle of attack. This is presented on the left of **Figure 8**.

There are two systems for loading in the part of the test bench intended for rigidity testing. The difference is in the nature of the load. When the flexural rigidity testing is performed, we load the blade with the force, while for torsional rigidity it is necessary to load the blade with coupling of forces.

Introducing force is performed by means of specially made system that consists of supporting structure, pulley, reductor unit, and engine with frequent control. The maximum force possible that can be achieved with this system is 2500 daN (**Figure 9**).

The rotor blade is loaded in six sections by lyres and measured from the place of the blade clamp (**Figure 10**, **Table 1**).

The introduction of coupling of forces on the blade, in order to get torsional rigidity, is performed in the way presented in **Figure 11**. In the relevant cross-section of the blade, the size of the required torsional moment is defined, which would cause a twisting angle of one radian in relation to the cross-section in the root part of the blade. A coupling of forces with small magnitudes of the coupling moment is introduced to the blade via the lyre in order to remain in the domain of linearity. The weights of a known mass through the system of pulleys and a lyre that is positioned on the blade are acting on the opposing sides of the blade, forming a coupling of forces.

Figure 8.
Acceptance and mounting of the blades for rigidity testing (left) and fatigue testing (right).
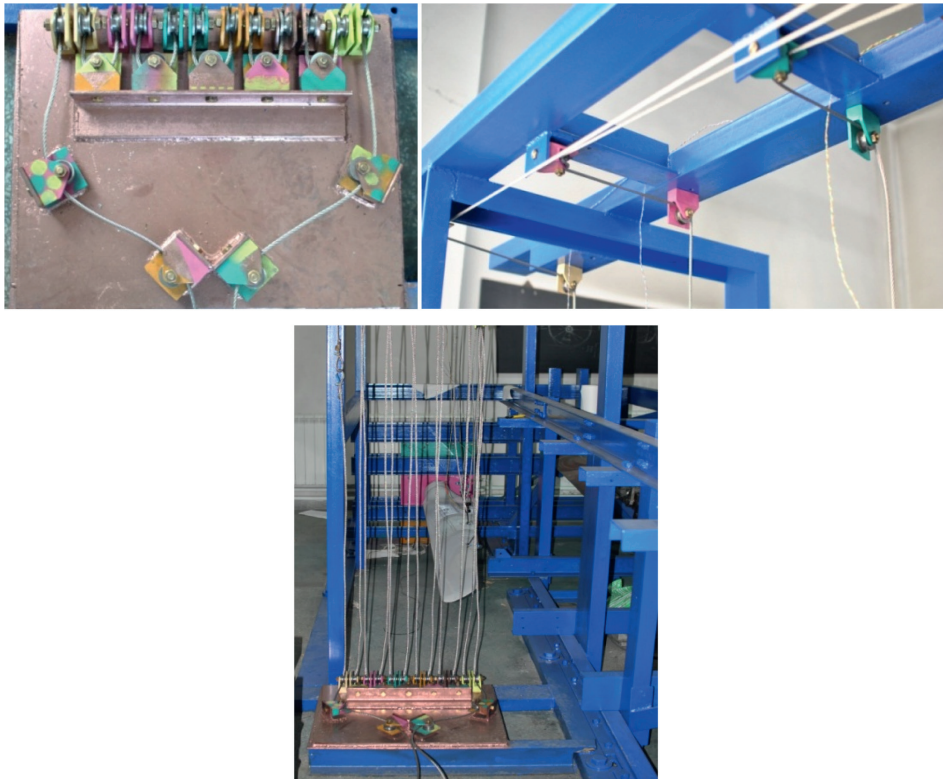
Figure 9.
Constriction for force distribution.

Figure 10.
Lyres for the force introduction.

Section	1	2	3	4	5	6
Distance (mm)	60.0	102.5	154.0	182.5	206.0	236.5

Table 1.
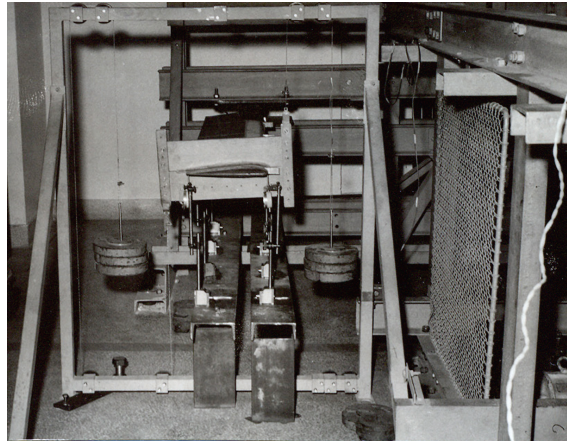*Positions of the six lyres for force introduction, measured from the place of the blade clamp.*

Figure 11.
Coupling of forces acting on a blade positioned on the test bench.

The acquisition chain in the case of flexural rigidity testing is consisted of a central acquisition unit, strain gauges, and displacement measuring device. The central acquisition unit HBM SPIDER 8 represents a multifunctional model of receiving analogue and digital signals with parallel tracing of the flow of input units, by means of integrated microcomputer, using higher-level system to relieve the acquisition route and to provide the flow of signals from certain 'smart sensors' directly to the control unit. SPIDER 8 is a multichannel acquisition unit designed for dynamic parallel measuring. Thanks to integration with personal computer as a higher-level system, the process of measuring is remarkably simple, and the total acquisition system is compact and of small dimensions (**Figure 12**).

The SPIDER acquisition unit offers 9600 measurements per second for each channel, with a resolution of 16 bits. All eight A/D converters operate simultaneously, converting physical values into digital signals in real time. For this experiment, two modules are utilized, providing a total of 16 measurement values.

Figure 12.
Two modules of SPIDER 8 and inductive displacement sensor LVDT—HBM.

The movement of a selected spot on the rotor blade is measured using a standard inductive displacement device, the LVDT model from HBM, with an accuracy class of ±0.2% and a measurement range of ±1 to ±500 mm (see **Figure 12**).

Six specially designed force sensors are used for measuring force. Each sensor consists of four strain gauges attached to its body as shown in **Figure 13**. The two strain gauges oriented in the axial direction measure the deformation of the sensor body under load, while the other two gauges, positioned crosswise, compensate for bending deformations. This setup ensures that the measured value is proportional only to the axial load.

Each force sensor (**Figure 14**) is connected to a Wheatstone full measuring bridge. The bridge is powered by a direct input voltage V1, while the output voltage V0 varies based on the resistance changes in the strain gauges R1, R2, R3, and R4 due to deformation. This output voltage is proportional to the axial force applied to the sensor. The arrangement of the strain gauges in the measuring bridge effectively compensates for the effects of bending moments on the output voltage.

The acquisition system for the torsional rigidity testing presented here is not so contemporary. The displacements of the measuring points in a predetermined layout were measured with comparators (**Figure 15**). The value of the torsion angle along its span is determined by means of the measured deflection values on the blade's leading and trailing edges.
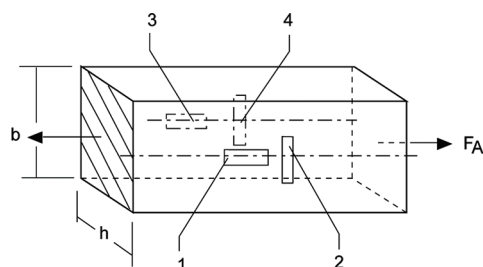

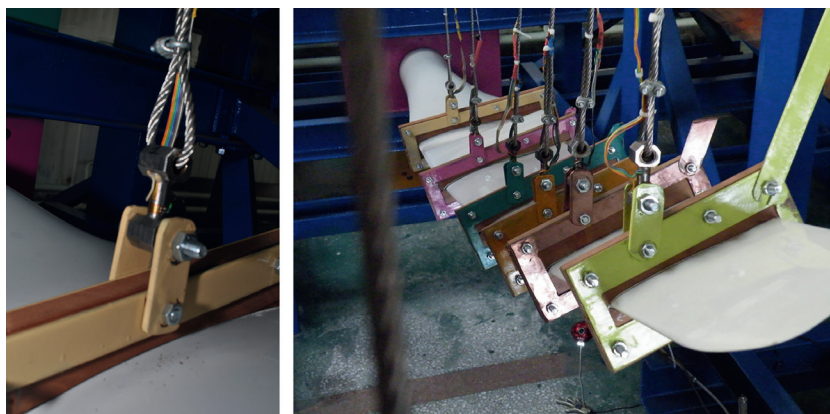**Figure 13.**
Schematic of force sensor.

Figure 14.
Force sensor on the blade and positioning on the blade.
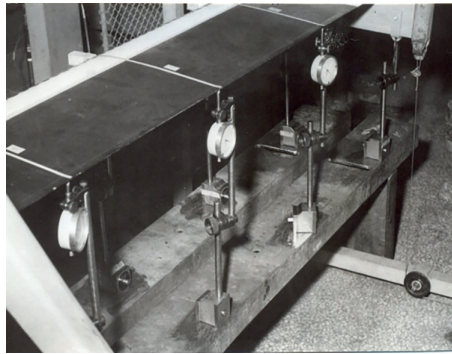
Figure 15.
Displacement measurement via comparators in a torsional rigidity testing.

The determination of flexural rigidity is demonstrated on an example of the Scirocco rotor blade—a 5.6 m diameter rotor (**Figure 16**). The rotor blade mass is 11.9 kg. Design and calculations have been made according to IEC 61400 design rules [7, 8].

The rotor blade failure is marked with the resulting force of 490.76 daN under maximum deflection of 27.999 mm. After the testing is completed, some separations are recorded, as presented in **Figures 17** and **18**.
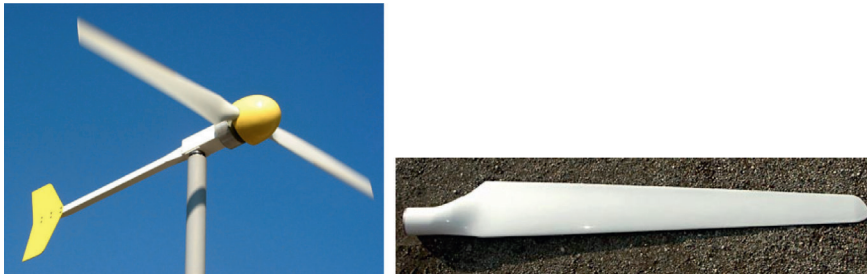

Figure 16.
Wind turbine Eoltec Scirocco and blade W55RBVS.

Figure 17.
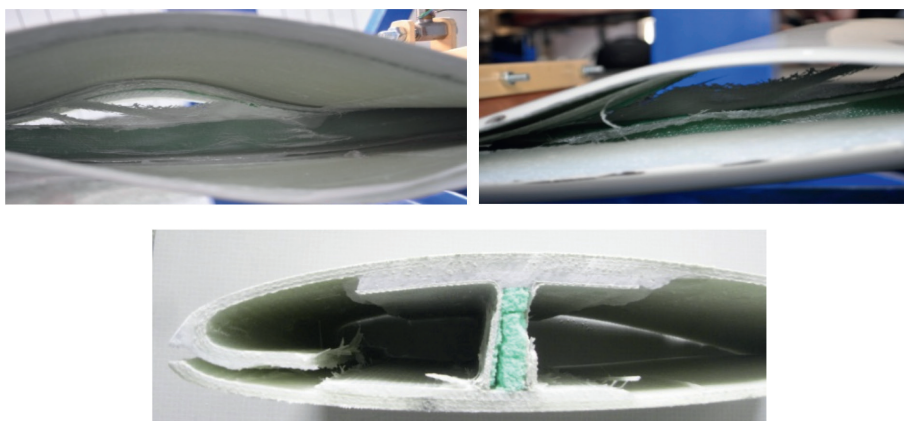*Position of the blade fracture.*

Figure 18.
Layering blades at the fracture.

Figure 19 shows the load applied to each sensor and the cumulative load on the rotor blade that resulted in its fracture. This represents the maximum load that the rotor blade can endure.

Next, we present the results of torsional rigidity testing for the tail rotor blade of the MI-8 helicopter, which is primarily a metal structure in its basic version. The composite blade of the MI-8 tail rotor serves as a long-term test sample at the Aviation Institute of the Faculty of Mechanical Engineering in Belgrade [9, 10]. It has successfully completed all testing stages outlined by this methodology. **Figure 20** shows the cross-sections where the torsional rigidity will be experimentally determined.

The measured values of torsional rigidity in four cross-sections of a rotor blade are presented in **Figure 21**. It is obvious the influence of the root of the blade on its torsional rigidity in cross-section 1. This test is performed in an elastic area of the blade's material. There is a possibility of determining the coupling of forces value that will lead to the failure of the rotor blade, which was not done in the presented case.

3.2 Fatigue test

On the right side of **Figure 8**, the setup for the blade prepared for bump or fatigue testing is shown. The connection is made using two plates and a double spindle with a trapezoidal thread. The angle of attachment of the blade is adjustable, with the front plate marked for the angle of attack, and the front nut secures the blade in place.
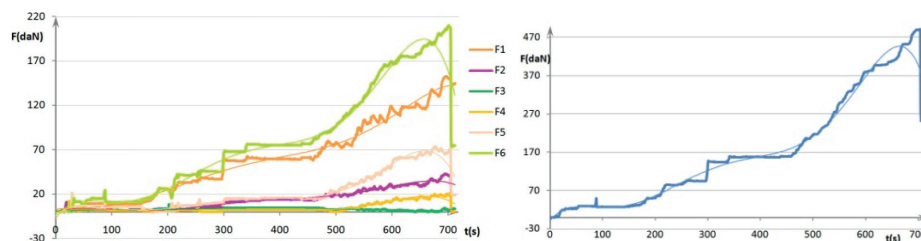

Figure 19.
Load distribution of each section in function of time and resulting force distribution in function of time.
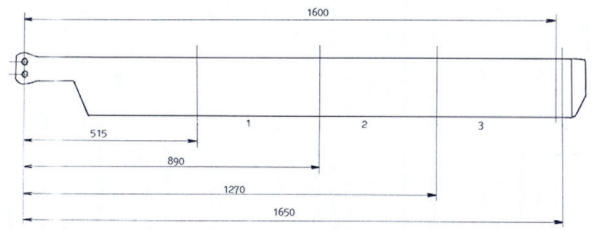
Figure 20.
Cross-sections on the rotor blade for torsional rigidity testing.
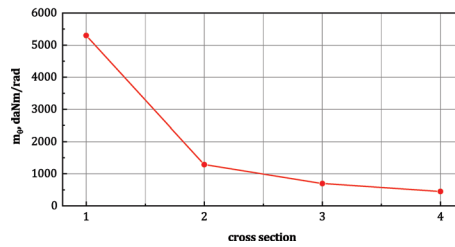

Figure 21.
Experimental results of torsional rigidity in four cross-sections.

The connection is fully secured against unscrewing with the back plate and nut. Additionally, a lever and pulley provide extra security against rotation in the clamping plane.

We will present the results of fatigue testing for the tail blade of the MI-8 helicopter, made from composite material at our Institute. The fatigue test bench features a hydraulic system for applying axial load to the blade, which includes a hydraulic cylinder, pressure gauges, an oil distribution system, and a pump with a drive motor. This test bench is a unique solution designed and implemented in the wind tunnel laboratories of the Faculty of Mechanical Engineering at the University of Belgrade. A schematic of the test bench is shown in **Figure 22**.

The static load is simulated by a centrifugal force of 11,350 daN, which results from the inertial characteristics of the blade at a nominal speed of 1100 RPM, and is applied using a hydraulic cylinder. The registration of this centrifugal force is facilitated by a strain gauge, a measuring bridge, and a suitable acquisition system. The strain gauges are attached to the transducer and configured in a full Wheatstone bridge (**Figure 23**) to enhance sensitivity and provide temperature compensation. Calibration of the measuring system was performed up to 20,000 daN using an
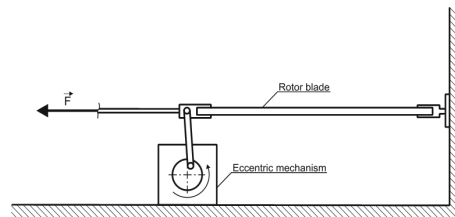

Figure 22.
Schematic of the test rig for fatigue testing.

Figure 23.
Integrated strain gauges (left) and reference force transducer (right).

HBM-calibrated inductive transducer, which has satisfactory measurement uncertainty (**Figure 23**). The SPIDER 8 served as the central acquisition unit for this testing, with its characteristics described previously.

The driving force simulating the alternating load is 500 daN, determined primarily by the aerodynamic characteristics of the blade, and acts normal to the plane of rotation. The registration of the excitation force is carried out in the same manner as the centrifugal force measurement, using strain gauges connected in a full Wheatstone bridge and an acquisition system. The strain gauges are attached to the excitation lever that connects the eccentric to the blade. The value of the excitation force is adjusted using an eccentric with variable eccentricity. Calibration of the strain gauges for an excitation force of 600 daN is performed on a special scale with a lever transmission ratio of 1:10. The frequency of the excitation force changes at 6.5 Hz (390 RPM), and the test is conducted at an angle of attack of 18°.

With the simultaneous application of these forces during the fatigue test, a total of 1500,000 cycles will be conducted at a frequency of 6.5 Hz. Following this, the relaxation phase will involve 1500 relaxations of the static centrifugal force, varying from 0 to 11,350 daN, in accordance with the guidelines outlined in the relevant document [11].

Due to the nature of the simulated load, continuous monitoring and control were conducted through the acquisition system's displays. The frequency of the excitation force was checked and adjusted at the beginning and end of each testing period. Before testing commenced, a thorough inspection of the tail rotor blade was performed. Additionally, careful monitoring of the blade's behavior took place throughout the test. No signs of delamination in the composite structure were observed during this time. Following the test program, a detailed inspection of the blade revealed no traces of damage, degradation, or changes in shape or structure, confirming that no delamination had occurred.

The fatigue test of the rotor blade demonstrated that it is capable of performing all its essential functions on the helicopter. This composite material rotor blade successfully endured the entire test program under all relevant loads, confirming the quality of the manufacturing technology used for the tail blade with composite materials.

3.3 Bump test

The bump test is conducted to determine the natural frequencies (frequency characteristics) of the examined blade. This test involves impulse excitation and

measuring the blade's response. The excitation is achieved by delivering a short impact with a hammer to the blade. For expected natural frequencies below 5000 Hz, a rubber hammer is recommended, while a plastic or wooden hammer is suitable for higher frequencies; thus, a rubber hammer was used in this case. It is important to ensure that the impact is brief enough to avoid damping the free oscillations that occur afterward. The free blade, mounted as it would be on a helicopter rotor, oscillates at all its natural frequencies following excitation. By recording displacement, velocity, or acceleration in the time domain and transforming these measurements into the frequency domain, the natural frequencies of the blade can be obtained. For this test, HBM accelerometers were used, placed at one-third intervals along the length of the blade (**Figure 24**), in conjunction with the SPIDER 8 acquisition system previously discussed in this chapter.

The connection between the time and frequency domains is illustrated in **Figure 25**. The complex signal in the time domain consists of two sinusoids with

Figure 24.
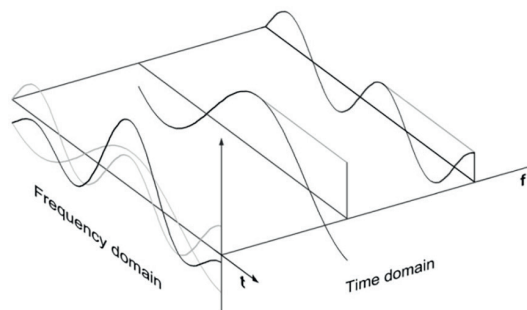*Position of the accelerometers.*

Figure 25.
Connection between the time and frequency domains.

different frequencies. By plotting the amplitude values of these sinusoids on the frequency axis, the representation of the signal in the frequency domain is obtained.

In our case, frequency (spectral) analysis is performed using Fourier analysis, which is based on the assumption that every periodic signal can be divided into a certain number of sinusoids, the sum of which is actually the signal we are observing. In contrast to continuous signals for which integral Fourier transformation (IFT) is used for analysis, discrete Fourier transformation (DFT) is used for discrete signal analysis. Fast Fourier transformation (FFT) is an algorithm that allows a computer to quickly perform a discrete Fourier transformation. Since the continuous signal coming from the transmitter is converted in the A/D converter into a discrete signal which is then analyzed in the computer, DFT was used for frequency analysis, that is, the algorithm for its calculation FFT. **Figure 26** presents the results of bump tests at different blade loads.
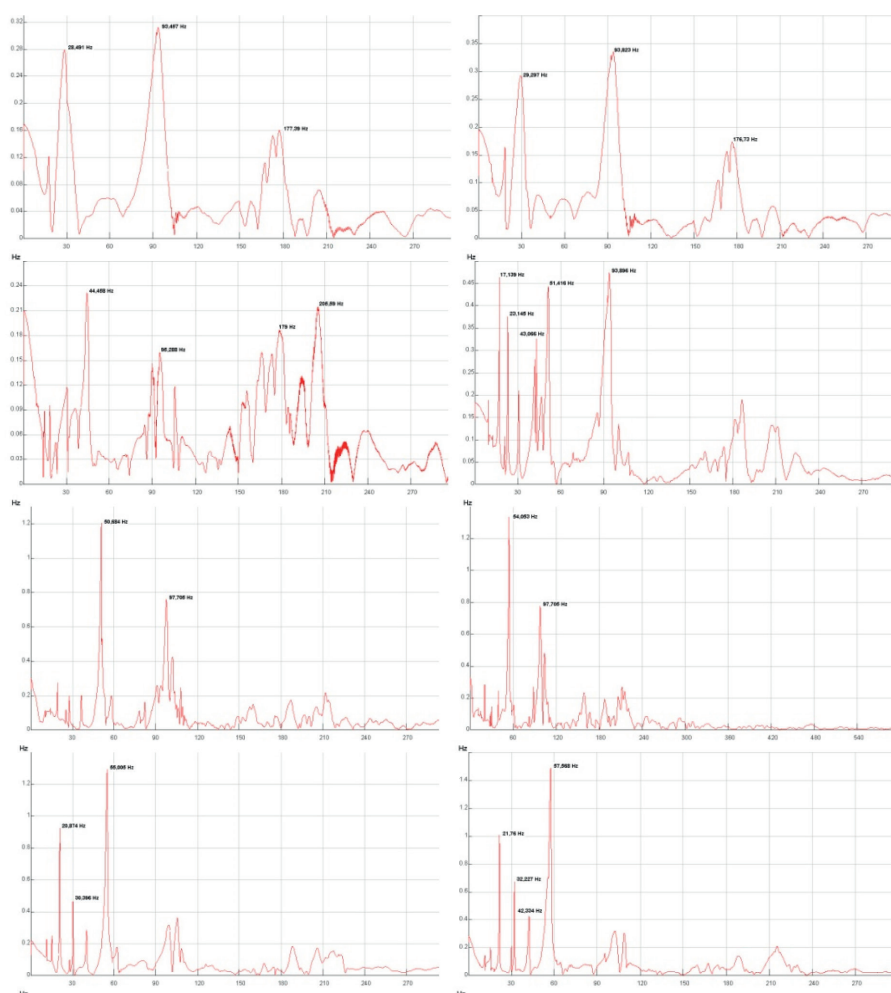

Figure 26.
Bump test results: (a) before testing, (b) load of 23,200 N, (c) load of 50,500 N, (d) load of 80,800 N, (e) load of 98,800 N, (f) load of 103,800 N, (g) load of 121,900 N, and (h) after unloading.

4. Structural testing by AFM/MFM mode

This research utilizes atomic and magnetic force microscopy to examine differences in surface topography and magnetic properties between sections of a rotor blade subjected to varying mechanical loads during rigidity testing. These findings could offer new insights into the material structure of rotor blades and potentially enhance their mechanical performance. The impellers were subjected to critical loads until failure, and sections from both critically and sub-critically loaded areas of the rotor blade are analyzed using magnetic force microscopy (MFM). MFM enables the characterization of surface and near-surface internal structures of samples, which is employed in this study to analyze structural changes in materials under different loads. The study presents results and compares the microstructures of two segments of the wind turbine blade. Additionally, atomic force microscopy (AFM) was employed to observe the surface morphology of the composite samples [12].

In this study, the scanning probe microscope utilized is the SPM-5200 by JEOL, Japan. Typically, deflection is measured by directing a laser spot onto the top surface of the cantilever, which is then reflected into an array of photodiodes. TappingMode AFM represents a more recent advancement where the imaging probe undergoes vertical oscillation at or near the resonant frequency of the cantilever (see **Figure 27**). Electromechanical feedback is employed to maintain constant oscillation amplitude during scanning. The resulting image is generated by mapping the vertical distance maintained by the scanner at each lateral data point to preserve the constant oscillation amplitude (see **Figure 28**). A significant advantage of TappingMode is its ability to eliminate lateral shear forces inherent in contact mode, which can potentially damage the structure being imaged, particularly on delicate specimens.

Magnetic force microscopy (MFM) is a derivative imaging mode based on TappingMode AFM, which maps the magnetic force gradient above the sample surface (refer to **Figure 29**). Unlike traditional AFM, MFM employs a probe tip coated with a thin layer of ferromagnetic material. This specialized tip reacts to magnetic domains present on the sample surface.

To obtain an image of the sample, MFM utilizes a two-pass technique. During the initial scan, the topography of the sample is mapped out. In the subsequent scan, the tip-sample distance is increased, and the biased tip is scanned along the topographical features obtained from the first scan. This second scan ensures that the tip maintains a constant distance from the sample surface, corresponding to the line of constant van der Waals force.

During the second scan in magnetic force microscopy (MFM), the tip follows the topographical line while maintaining a constant van der Waals force. This ensures that changes in the signal primarily reflect variations in magnetic force. The evaluation of
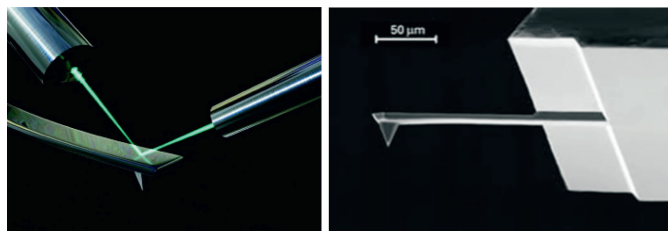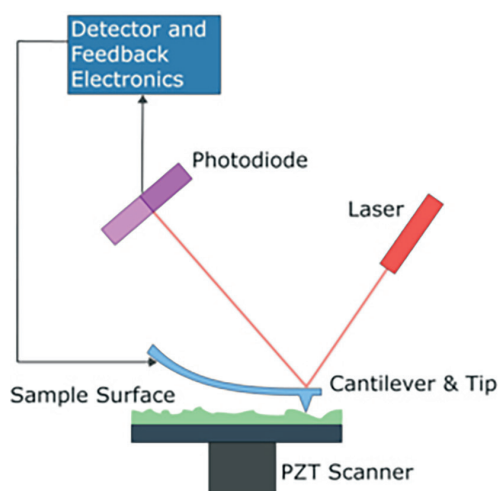

Figure 27.
Cantilever with a sharp tip (probe).
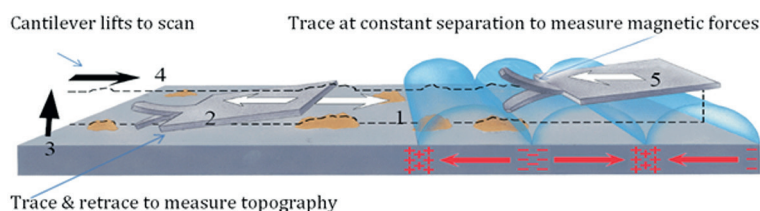
Figure 28.
Schematic of a laser measurement.

Figure 29.
LiftMode for topography and magnetic force gradient measurement.

magnetic properties relies on the magnetic force gradient image, which qualitatively depicts the distribution of magnetic fields across the scanned area, indicating local variations in magnetic properties.

The cantilever used in this study is manufactured by MikroMasch (Estonia) under the trade name NCS18 Co-Cr. The MFM probe features a silicon etched tip with a conical shape, coated with layers of Co and Cr. As a result of the coating, the tip has a radius of approximately 90 nm. The full cone angle of the tip is 40°.

It is anticipated that the less loaded portion of the material (Sample 1, depicted in **Figures 30** and **31**) will exhibit lower surface roughness. This is because the layers of silicone fibers held by epoxy are expected to be more uniformly aligned under lower stress conditions. AFM analysis reveals that Sample 1 has an average surface roughness (Ra) approximately 200 nm smaller than Sample 2, which experienced higher loads during wind turbine testing. This suggests that the inner layers of Sample 2 may have undergone deformation, potentially resulting in misalignment compared to their original state.

From the magnetic characteristic figures, it is evident that Sample 1 displays a relatively uniform distribution of magnetic properties, whereas Sample 2 exhibits 'black dots'. These 'black dots' signify abrupt changes in sample magnetization, indicative of variations in magnetic field gradients. The presence of these features on the figure of Sample 2, which was subjected to higher loads (as shown in **Figure 32**), suggests
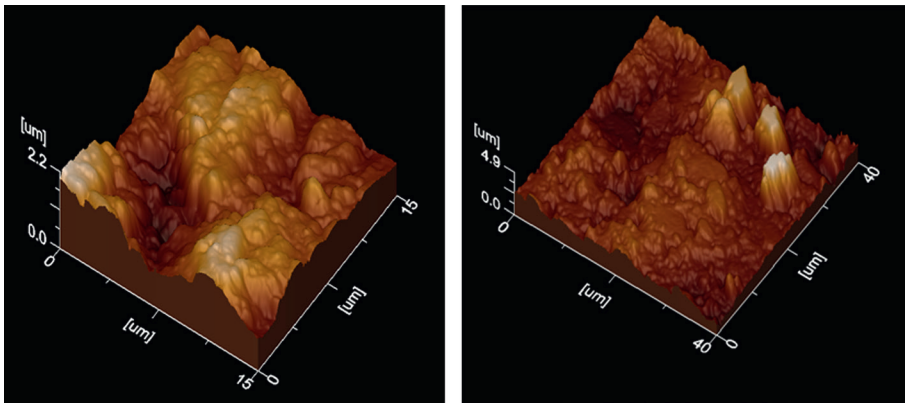
Figure 30.
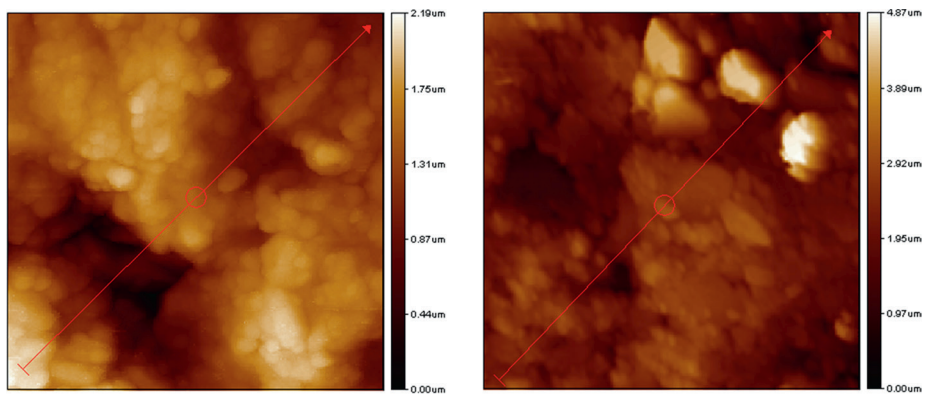*Surface roughness for less loaded (left) and more loaded (right) sample.*

Figure 31.
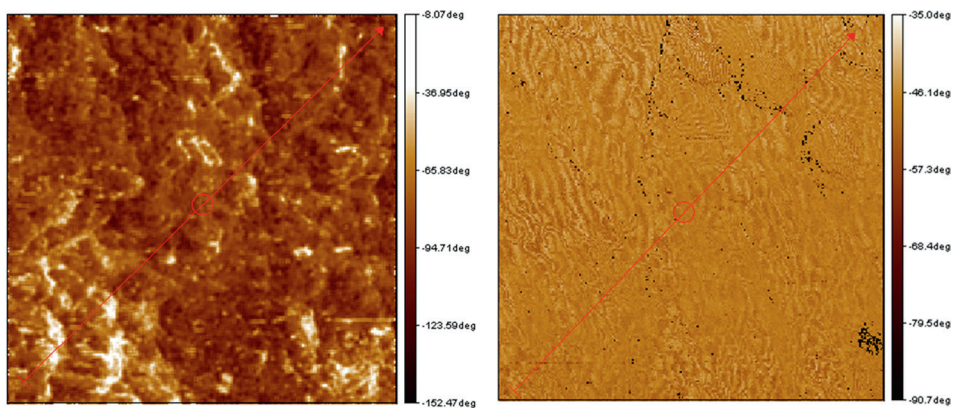*Detail of surface roughness for less loaded (left) and more loaded (right) sample.*

Figure 32.
Magnetic characteristics of the material: left—less loaded, right—more loaded.

potential alterations in the material's structure and stratification due to the applied loading conditions.

Research using atomic and magnetic force microscopy indicates that samples taken from areas under higher loads exhibit the expected characteristics of increased surface roughness and height differences. Additionally, the presence of 'black dots' or 'magnetic holes' suggests internal stratification within the composite material. Overall, these findings from the experiment confirm that the tested rotor blade demonstrates very high rigidity.

5. Conclusions

In this chapter, methodology for testing a rotor blades made of composite material is presented. It involves performance and mechanical testing. These tests are needed, either in the course of design or at the end of production of a rotor blade. Presented example for performance testing proves that the test bench for performance testing can be used both for testing the traction-dynamic characteristics and for propellers' balancing. Test bench for rigidity testing can be used in the area of elastic deformations of the rotor blades, hence determining the flexural/torsional rigidity of the blade on the test. However, it can be used to experimentally determine the maximum force/coupling of forces that the blade on the test can withstand before the failure. In this chapter, we have presented determination of torsional rigidity (elastic area of deformation) and maximum force that led to destruction of the rotor blade. Test bench for fatigue testing is also presented. Bump test reveals at what frequencies the rotor blade should not be operating on. The rigidity tests should be complemented with atomic and magnetic force microscopy to discern variations in surface topography and magnetic properties among different sections of the rotor blade subjected to varying mechanical loads.

Presented methodology can be applied for rotor blades of any size, depending on the available hardware on the site. Of course, for extremely large structures, one can apply the similarity theory and dimensional analysis. The acquisition system is simple and the same, independently on the size of the test bench.

Author details

Goran Vorotović[1*], Jela Vorotović[1], Nebojša Petrović[1], Nikola Davidović[1], Đorđe Novković[1] and Pavle Petrović[2]

1 Faculty of Mechanical Engineering, University of Belgrade, Belgrade, Serbia

2 Civil Aviation Directorate of the Republic of Serbia, Belgrade, Serbia

*Address all correspondence to: gvorotovic@mas.bg.ac.rs

IntechOpen

References

[1] Armstrong KB, Barrett RT. Care and Repair of Advanced Composites. 1st ed. Warrendale, PA, USA: SAE International; 1998

[2] Hoskin BC, Baker AA. Composite materials for aircraft structures. In: AIAA Education Series. 1st ed. New York: AIAA Inc.; 1986

[3] Adams DO, Kearney HL. Full-scale fatigue testing of advanced fiber composite components. Journal of the American Helicopter Society. 1986;**31**:66-72. DOI: 10.4050/JAHS.31.66

[4] Curtis PT. The fatigue behaviour of fibrous composite materials. The Journal of Strain Analysis for Engineering Design. 1989;**24**(4):235-244. DOI: 10.1243/03093247V244235

[5] Mitrović Č, Petrović N, Bengin A, Bekrić D, Dragović V, Simonović A, et al. Structural testing of small wind turbine blade up to failure. In: International Conference on Innovative Technologies. Conference IN-TECH 2011, Bratislava, CTU – Czech Technical University in Prague. 2011

[6] Vorotović G, Burazer J, Bengin A, Mitrović Č, Januzović M, Petrović N, et al. A case study of a methodological approach to the verification of UAV propeller performance. Strojniški Vestnik—Journal of Mechanical Engineering. 2023;**69**(5-6):199-207. DOI: 10.5545/sv-jme.2022.432

[7] International Standard IEC 61400- 2. Wind Turbines – Part 2: Design Requirements for Small Wind Turbines. Switzerland: International Electrotechnical Commission; 2019

[8] International Standard IEC 61400-1. Wind Turbines - Part 1: Design Requirements. Switzerland: International Electrotechnical Commission; 2019

[9] Rasuo B. Design, fabrication and testing of the helicopter tail rotor blade from composite laminated materials. In: 13th International Conference on Composite Materials, ICCM-13. Beijing, China: International Committee of Composite Materials; 2001

[10] Rasuo B. Testing of the Survivability of an Aeronautical Constructions from Composite Materials, SAE/AIAA 1999- 01-5597. In: World Aviation Congress. San Francisco, California: SAE International; 1999

[11] Rasuo B. Helicopter tail rotor blade from composite materials: An Experience. SAE International Journal of Aerospace. 2011;**4**(2):828-838. DOI: 10.4271/2011-01-2545

[12] Yahya N, Kashif M, Daud H, Mohd Zaid H, Shafie A, Nasir N, et al. Fabrication and characterization of Y3.0-XLaXFe5O12 PVA composite as EM waves detector. International Journal of Basic & Applied Sciences IJBAS—IJENS. 2009;**9**(9):131-134